UC Irvine
UC Irvine Previously Published Works

Title

Respiratory self-gating for free-breathing magnetization transfer MRI of the abdomen.

Permalink

Journal

ISSN

Authors

Li, Weiguo
Zhang, Zhuoli
Li, Kangan
et al.

Publication Date

DOI

Peer reviewed

Respiratory Self-Gating for Free-Breathing Magnetization Transfer MRI of the Abdomen

Weiguo Li[1], **Zhuoli Zhang**[1], **Kangan Li**[1], **Ning Jin**[2], **Yue Zhang**[1], **Tianjing Zhang**[1,3], **Frank H. Miller**[1], and **Andrew C. Larson**[1,3]

[1]Department of Radiology, Northwestern University, Chicago, Illinois, USA

[2]Siemens Healthcare, Columbus, Ohio, United States

[3]Department of Biomedical Engineering, Northwestern University, Chicago, Illinois, USA

Abstract

Purpose—Magnetization transfer (MT) MRI can be effective for the diagnosis of a broad range of fibrotic diseases including liver fibrosis. However, respiratory motion, a major source of artifacts in thoracic and abdominal MR imaging, can obscure important anatomic structures, making diagnosis difficult. In this study, we explored the potential to combine free-breathing (FB) respiratory self-gating (RSG) methods with MT saturation for FB MT ratio (MTR) measurements of abdominal organs.

Methods—A respiratory self-gated multiple gradient recalled echo sequence with MT pre-saturation (RSG-MT GRE) was developed and applied in a series of seven normal volunteers. We compared the MTR values of liver, pancreas, kidney, spleen, and posterior paraspinal muscle measured using our RSG-MT GRE sequence and a conventional MT GRE sequence.

Results—RSG consistently reduced motion artifacts within MT weighted images acquired during FB, improved the accuracy of FB MTR measurements, and produced comparable MTRs to breath-holding MTR measurements.

Conclusion—RSG approaches may offer to improve the utility of MT weighted imaging methods for the assessment of fibrotic diseases and tumor desmoplasia in abdominal organs.

Keywords

Magnetization transfer; Respiratory self-gating; Respiratory motion; abdomen

Introduction

Abnormal and exaggerated deposition of extracellular matrix is a hallmark of tumor associated desmoplasia (1) as well as many fibrotic diseases, such as liver fibrosis (2) and renal fibrosis (3). It has recently been reported that these excessive amounts of extracellular

matrix proteins in fibrosis tissues can be detected with magnetization transfer (MT) MRI techniques (4,5). MT is a dynamic process involving the exchange of magnetization between sub-populations of free water protons and those water protons bound to macromolecules (6,7). MT MRI techniques have been utilized in study of neurological diseases, such as multiple sclerosis (8), Alzheimer's disease (9), as well as *in vivo* studies in animal models of cancer (10) and Crohn's disease (5). However, the application of MT techniques in abdominal diseases has been limited, potentially due to the artifacts commonly caused by motion of the abdominal organs.

Respiratory motion is a major source of artifacts in thoracic and abdominal MR imaging. It can lead to significant image quality deterioration and inaccurate measurements. Multiple techniques have been developed to suppress or compensate respiratory motion artifacts during MRI acquisition. These include breath-holding (BH), respiratory gating, k-space view reordering, and respiratory navigation techniques. Though BH is commonly employed to eliminate respiratory motion artifacts, overall slice coverage and spatial resolution are limited by the requisite BH duration. For severely ill patients or those under sedation, it can be difficult to comply with BH commands. Alternative free-breathing (FB) techniques could be useful to reduce motion artifacts and avoid patient compliance issues while providing accurate MRI measurements with sufficient spatial coverage. Typically reliant upon real-time monitoring of respiratory cycles, most FB acquisition methods use an external physiological monitoring device such as pneumatic bellows to monitor respiratory motion (11). Though required no changes to the image reconstruction algorithm, these respiratory synchronization and compensation methods require patient cooperation or commonly substantial modifications to the data acquisition strategy. Commonly used bellows signals are highly susceptible to hysteresis and representative of respiratory motion patterns of the chest wall rather than the direct respiratory motion patterns of the internal tissues of interest. Respiratory navigator gating techniques provide greater accuracy than respiratory bellows gating without the need for additional gating equipment (12,13). However, navigators inherently disrupt magnetization and resulting image signal from abdominal tissues given that typically the diaphragm is tracked during these procedures. Additionally, the motion measured by the navigator strongly depends on where it is placed (14). Recently, respiratory self-gating (RSG) approaches have demonstrated the potential to acquire images during FB while avoiding respiratory motion artifacts in both cardiac and abdominal imaging applications (15–17). These methods typically involve acquiring an additional RSG signal in the k-space center for respiratory synchronization without using any external tracking device or requiring additional gradients or radiofrequency pulses disruptive of steady-state imaging conditions. Most recently RSG techniques have been used for accurate FB abdominal phase-contrast flow and T_2^* measurements (18).

In this work, we explored the potential to combine RSG methods with MT saturation for FB MTR measurements. To demonstrate the feasibility of the newly proposed methods, a RSG-MT gradient echo (GRE) sequence was developed to permit the application of a MT pre-saturation pulse and the acquisition of both the RSG signal and imaging data during each repetition time. We compared the MTR values of liver, pancreas, kidney, spleen, and

posterior paraspinal muscle measured using our RSG-MT GRE sequence and a conventional MT GRE sequence.

Methods

MRI sequence

The RSG-MT sequence was derived via the modification of a standard 2D gradient echo (GRE) sequence to permit the application of a MT pre-saturation pulse and the acquisition of both the RSG signal and imaging data during each repetition time. A small time delay (T_{RSG} = 80 μs) was added after the slice-selective refocusing gradient (Fig. 1a). RSG data points, mapped to k-space center, were collected during T_{RSG} before phase-encoded imaging data acquisition. A segmented phase-encoding method was used to repeatedly acquire multiple adjacent k-space lines (segment acquisition repeated over period anticipated to cover an entire respiratory cycle) (18).

Volunteer studies

Volunteer studies were performed using a 1.5 T clinical MRI scanner (Magnetom Espree, Siemens Medical Solutions, Erlangen, Germany). A body matrix array and spinal array coils were used for MRI signal reception. Seven healthy volunteers were enrolled (four males, three females, age: 34 ± 10, BMI: 22.6 ± 3.3). The Institutional Review Board approved this study and informed consent was obtained from all volunteers.

MR imaging was first performed using the conventional MT-GRE sequence during BH at expiration (BH-MT) with and without MT saturation. Then, another set of free-breathing MT (FB-MT) GRE images were acquired during FB using same scanning parameters. Last, the respiratory self-gated MT (RSG-MT) GRE images during free breathing were acquired. For all the scans with MT saturation, a Gaussian RF pulse was applied with pulse length of 10 ms, flip angle (FA) of 900°, and off-resonance frequency of 1.5 kHz. Due to the small time delay (T_{RSG} = 80 μs) added after the slice-selective refocusing gradient (Fig. 1a), TE of RSG-MT sequence was 2.58 ms with 80 μs longer than TEs of the other two methods (TE = 2.5 ms). Other imaging parameters identical in each of the three sequences were: TR = 40 ms, FA = 15°, bandwidth = 400Hz/pixel, matrix = 128×128, slice thickness = 5 mm, field of view (FOV) = 350×350 mm^2, number of slices = 1. For segmented phase-encoding, 32 phase lines for each segment were acquired with the RSG-MT sequence. The typical RSG-MT acquisition time was 42 seconds. The BH-MT and FB-MT acquisition duration were 14 seconds. For FB-MT and RSG-MT scans, volunteers were instructed to breath evenly and consistently during the scan. Higher-resolution RSG-MT scans were also carried out with in-plane resolution of 1.82×1.82 mm^2, matrix = 192×192, and other scan parameters same as those described above. The acquisition time for higher-resolution RSG-MT scan was 4.14 minutes.

Data analysis

RSG-MT images were reconstructed offline using the MATLAB software (MathWorks, Natick, MA). RSG data points collected prior to phase-encoded imaging data acquisition were used to extract the respiratory signal. Respiratory gating signal was constructed based

on the mean phase of data points collected during T_{RSG} sampling period. These RSG data points were collected from RF receiver coil located nearest the imaging slice, though k-space data collected from the multiple coils were used for the final image reconstruction. K-space lines acquired corresponding to RSG signal phases below a local threshold were selected for inclusion in the retrospectively synchronized reconstruction. MTR maps were generated voxel-wise using the following equation $100 \times (1 - M_{sat}/M_0)$, where M_{sat} represents the signal intensity for reconstructed image acquired following application of the MT pulse, M_0 is the signal intensity of image acquired without MT saturation.

Image Quality Analysis

Qualitative comparisons were made between images obtained with BH-MT, FB-MT, and RSG-MT to evaluate the effectiveness of using RSG method to mitigate abdominal respiratory motion. The MT weighted images with each of the three techniques were displayed simultaneously along the three rows. The order of display was randomized with regard to the acquisition methods. To evaluate overall image quality based on the artifact level in the liver, two experienced radiologists (with greater than 10 years experience reading abdominal MR) blinded to the image acquisition strategies scored the images together by consensus according a scoring system from 1 to 4. In this scoring system, "1" indicated poor with severe artifacts precluding organ visualization; "2" indicated acceptable with many artifacts limiting interpretation; "3" indicated good with limited artifacts that are limited bearing on interpretation; "4" indicated excellent with no apparent artifacts.

Statistical Analysis

For each volunteer, region of interests (ROIs) were drawn within liver, pancreas, kidney, spleen, and posterior paraspinal muscle for comparison between the three techniques. Mean MTR values within the ROIs from BH-MT images were compared with the counterparts from RSG-MT and FB measurements using a pairwise Student's t-test with significance level of 0.05. The percentage errors of RSG-MT and FB MTR measurements were also calculated according to the following two equations: $100 \times (MTR_{RSG} - MTR_{BH})/MTR_{BH}$ and $100 \times (MTR_{FB} - MTR_{BH})/MTR_{BH}$. The MTR results were further analyzed using the Bland–Altman method to compare the agreement between the three methods. Comparisons between mean MTRs measured with BH-MT, FB-MT and RSG-MT approaches were also performed with linear regression analysis using BH MTR results as the standard. The scores of overall image quality for BH-MT, FB-MT and RSG-MT were compared using pair-wise Wilcoxon signed rank tests with a significance level of 0.05.

Results

Fig. 1b shows a representative segment of RSG signal recorded in one volunteer. The blue dots represent the RSG signal with signal phases below the local threshold corresponding to the anticipated expiration position. k-Space lines acquired during the same TR corresponding to RSG signal phases below the local threshold were selected for inclusion in the subsequently reconstructed images.

Representative MT-weighted images acquired using BH, FB and RSG techniques in caudal liver positions are shown in Fig. 2a–c. The corresponding MTR maps for each imaging strategy are also shown in the right column in Fig. 2. Artifacts were clearly evident within the FB images (Fig. 2a). The RSG-MT method effectively mitigated respiratory motion artifacts (Fig. 2c), producing qualitatively similar images to that provided with BH approach (Fig. 2b). Correspondingly, an MTR map devoid of any apparent respiratory motion artifact was generated with images acquired using the RSG-MT method (right column, Fig 2c.). The qualitative image scoring provided via reviewers blinded to the acquisition strategies supported these findings. Image quality scores for BH-MT (2.93 ± 0.47) and RSG-MT (3.07 ± 0.47) were significantly superior to the scores for FB (1.43 ± 0.51, $P = 0.001$ for each paired comparison). There was no significant difference between the image quality scores for BH-MT and RSG-MT ($P = 0.41$). Fig. 2d shows representative higher-resolution images acquired without/with MT saturation with in-plane resolution of 1.82×1.82 mm^2 and acquisition time of 4.14 min along with the corresponding MTR map. No clearly apparent motion artifacts were observed for these images reconstructed from data acquired using the RSG-MT method.

Table 1 summarizes the resulting mean MTR measurements within the liver, pancreas, kidney, spleen, and posterior paraspinal muscle performed using the three implemented approaches. While comparable percentage error of MTRs from posterior paraspinal muscle was found between RSG MT (3.11 ± 2.24) and FB MT (3.35 ± 2.58), the percentage errors of MTRs from the liver, pancreas, kidney and spleen acquired using RSG-MT method are significantly smaller than those acquired using FB-MT method. A strong correlation was observed between RSG MTR and BH MTR measurements with correlation coefficient of $R^2 = 0.96$ ($P < 0.01$), while a weaker correlation was found between MTR measured during FB and BH ($R^2 = 0.82$; $P < 0.01$). As demonstrated in Bland-Altman plots (Fig. 3), RSG MTR showed better absolute agreement with the BH MTR measurements than FB MTR with BH MTR measurements. The pairwise Student's t-test indicated that there were no significant differences between BH MTR and RSG MTR measurements in each organ ($P = 0.27$), whereas FB MT methods significantly overestimated MTR values compared with BH measurements ($P = 0.002$).

Discussion and Conclusions

Respiratory motion can produce severe artifacts in abdominal GRE-based sequences and can lead to significant errors in GRE-based MTR measurements. Commonly, the BH approach is used to mitigate respiratory motion artifacts; however, overall spatial resolution and coverage is limited by the BH duration. Alternative FB MTR mapping approaches should be of value for a variety of quantitative abdominal imaging applications. The principle aim of this study was to demonstrate the feasibility of combining RSG techniques with MT GRE sequences for accurate MTR measurements during FB. In these initial studies, our RSG-MT GRE approach effectively eliminated respiratory motion induced artifacts in MT-weighted images, produced good image quality and accurate MTR measurements in liver, spleen, kidneys and posterior paraspinal muscle.

RSG MT techniques could permit data acquisition during FB and generation of MTR maps with limited respiratory motion artifacts. This can be critical during abdominal MTR mapping because respiratory motion not only deteriorates image quality, but also leads to inaccurate MTR measurements in tissues caused by, for example, misregistration of the two measured images for MTR calculation. To date, abdominal applications of MT MRI were primarily reported in the form of MTRs for determining the extent of hepatic collagen deposition in preclinical models of Niemann-Pick disease (19) and assessing degrees of hepatic fibrosis in chronic liver disease (20–22). However, the results of these prior abdominal imaging studies have been variable and relatively inconclusive regarding overall diagnostic efficacy (22). One possible reason could be that MTR measurements were confounded by variable degrees of hepatic steatosis and inflammation in hepatic imaging (5,20). One other reason could be simply that respiratory motion artifacts may aggravate the uncertainty of these measurements. Our RSG-MT approach, by mitigating respiratory motion artifacts, could mitigate these potentially important factors. RSG MT technique might also be more applicable for imaging abdominal tissues in ill patients or children who may struggle to comply with BH commands. Furthermore, the spatial resolution achievable with the RSG-MT approach could no longer be limited by BH duration. No clearly apparent motion artifacts were observed in the acquired higher resolution MT weighted images and the corresponding MTR map (Fig. 2d). Additionally, while quantitative magnetization transfer MRI (qMTI) with two-pool models has been applied for neurologic imaging applications, these methods have yet to be fully explored for abdominal imaging. The qMTI techniques use MT weighted images acquired at multiple offset saturation frequencies with signals fit to a two-pool model to provide measurements that more directly characterize the MT process (10,23). Multiple scans with a range of offset frequencies can require extensive scan times that could lead to image artifacts due to respiratory motion during abdominal studies. The RSG-MT approach, by eliminating respiratory motion induced artifacts in MT-weighted images, has shown the potential to extend the applications of two-pool model based qMTI techniques to the study of abdominal diseases. Further investigation of RSG qMTI technique in abdomen is ongoing.

There are several limitations of the proposed RSG-MT approach. First, in the current RSG-MT sequence, the RSG signal is collected at the beginning of each TR and before imaging data acquisition. Thus, the subsequent delayed TE could reduce SNR especially for relatively short T_2^* conditions. The prolonged TE also induces T_2^* weighting factor to the acquired images, thus mildly altering the MT weighting in these images. One approach to eliminate differences in MT weighting between methods could have been to acquire the BH, FB, and RSG scans all with same echo time by using the RSG pulse sequence. However, additional studies using, for example, spiral acquisition with a spiral-out readout of k-space (24) could enable shorter echo times for a given level of contrast. Second, rather than prospective gating, the retrospective gating approach used in this study could lead to redundant data acquisition and increased acquisition time. Also, insufficient data may be acquired at quiescent respiratory phases to ensure complete k-space datasets for image reconstruction if an insufficient acquisition window is chosen or the volunteer has inconsistent respiratory motion patterns. Further studies are necessary to optimize the acquisition window, phase encoding algorithm, and scanning protocol to improve efficiency

within clinical settings for patients with different disease conditions, especially with aberrant breathing patterns. Finally, further studies are also necessary to optimize the MT saturation RF pulse timing, power and offset frequencies, to validate the accuracy of RSG-MT techniques in a series of phantom and patient studies, to evaluate the trade-off between acquisition time and artifact levels and most importantly the reproducibility of this technique in clinical settings, and to evaluate the transferability of the sequence to other MRI scanners, especially scanners from other vendors.

In conclusion, we have demonstrated the feasibility of using RSG techniques to permit MTR measurements in the abdomen during FB image acquisitions. When compared with FB MTR measurements, RSG-MT could be able to effectively avoid artifacts caused by respiratory motion and produce comparable MTR measurements to BH MTR measurements in abdominal organs.

Acknowledgments

References

1. Olive KP, Jacobetz MA, Davidson CJ, Gopinathan A, McIntyre D, Honess D, Madhu B, Goldgraben MA, Caldwell ME, Allard D, Frese KK, DeNicola G, Feig C, Combs C, Winter SP, Ireland-Zecchini H, Reichelt S, Howat WJ, Chang A, Dhara M, Wang L, Ruckert F, Grutzmann R, Pilarsky C, Izeradjene K, Hingorani SR, Huang P, Davies SE, Plunkett W, Egorin M, Hruban RH, Whitebread N, McGovern K, Adams J, Iacobuzio-Donahue C, Griffiths J, Tuveson DA. Inhibition of Hedgehog Signaling Enhances Delivery of Chemotherapy in a Mouse Model of Pancreatic Cancer. Science. 2009; 324(5933):1457–1461. [PubMed: 19460966]

2. Hernandez-Gea V, Friedman SL. Pathogenesis of liver fibrosis. Annual review of pathology. 2011; 6:425–456.

3. Liu Y. Cellular and molecular mechanisms of renal fibrosis. Nature reviews Nephrology. 2011; 7(12):684–696.

4. Li W, Zhang Z, Nicolai J, Yang GY, Omary RA, Larson AC. Magnetization transfer MRI in pancreatic cancer xenograft models. Magn Reson Med. 2012; 68(4):1291–1297. [PubMed: 22213176]

5. Adler J, Swanson SD, Schmiedlin-Ren P, Higgins PDR, Golembeski CP, Polydorides AD, McKenna BJ, Hussain HK, Verrot TM, Zimmermann EM. Magnetization Transfer Helps Detect Intestinal Fibrosis in an Animal Model of Crohn Disease. Radiology. 2011; 259(1):127–135. [PubMed: 21324841]

6. Wolff SD, Balaban RS. Magnetization transfer contrast (MTC) and tissue water proton relaxation in vivo. Magn Reson Med. 1989; 10(1):135–144. [PubMed: 2547135]

7. Henkelman RM, Stanisz GJ, Graham SJ. Magnetization transfer in MRI: a review. NMR Biomed. 2001; 14(2):57–64. [PubMed: 11320533]

8. Ge Y, Grossman RI, Udupa JK, Babb JS, Kolson DL, McGowan JC. Magnetization transfer ratio histogram analysis of gray matter in relapsing-remitting multiple sclerosis. AJNR Am J Neuroradiol. 2001; 22(3):470–475. [PubMed: 11237968]

9. Bigot C, Vanhoutte G, Verhoye M, Van der Linden A. Magnetization transfer contrast imaging reveals amyloid pathology in Alzheimer's disease transgenic mice. Neuroimage. 2014; 87:111–119. [PubMed: 24188815]

10. Li W, Zhang Z, Nicolai J, Yang GY, Omary RA, Larson AC. Quantitative magnetization transfer MRI of desmoplasia in pancreatic ductal adenocarcinoma xenografts. NMR Biomed. 2013; 26(12):1688–1695. [PubMed: 23940016]

11. Bailes DR, Gilderdale DJ, Bydder GM, Collins AG, Firmin DN. Respiratory ordered phase encoding (ROPE): a method for reducing respiratory motion artefacts in MR imaging. J Comput Assist Tomogr. 1985; 9(4):835–838. [PubMed: 4019854]

12. Firmin D, Keegan J. Navigator echoes in cardiac magnetic resonance. Journal of cardiovascular magnetic resonance : official journal of the Society for Cardiovascular Magnetic Resonance. 2001; 3(3):183–193. [PubMed: 11816615]

13. Welch EB, Manduca A, Grimm RC, Ward HA, Jack CR Jr. Spherical navigator echoes for full 3D rigid body motion measurement in MRI. Magn Reson Med. 2002; 47(1):32–41. [PubMed: 11754440]

14. Stuber M, Botnar RM, Danias PG, Kissinger KV, Manning WJ. Breathhold three-dimensional coronary magnetic resonance angiography using real-time navigator technology. Journal of cardiovascular magnetic resonance : official journal of the Society for Cardiovascular Magnetic Resonance. 1999; 1(3):233–238. [PubMed: 11550357]

15. Brau AC, Brittain JH. Generalized self-navigated motion detection technique: Preliminary investigation in abdominal imaging. Magn Reson Med. 2006; 55(2):263–270. [PubMed: 16408272]

16. Jin N, Lewandowski RJ, Omary RA, Larson AC. Respiratory self-gating for free-breathing abdominal phase-contrast blood flow measurements. J Magn Reson Imaging. 2009; 29(4):860–868. [PubMed: 19306414]

17. Crowe ME, Larson AC, Zhang Q, Carr J, White RD, Li D, Simonetti OP. Automated rectilinear self-gated cardiac cine imaging. Magn Reson Med. 2004; 52(4):782–788. [PubMed: 15389958]

18. Jin N, Zhang Z, Zhang L, Lu G, Larson AC. Respiratory self-gated multiple gradient recalled echo sequence for free-breathing abdominal R2* mapping. Magn Reson Med. 2011; 66(1):207–212. [PubMed: 21695725]

19. Guo J, Erickson R, Trouard T, Galons JP, Gillies R. Magnetization transfer contrast imaging in Niemann pick type C mouse liver. J Magn Reson Imaging. 2003; 18(3):321–327. [PubMed: 12938127]

20. Komu M, Alanen A. Magnetization transfer in fatty and low-fat livers. Physiol Meas. 1994; 15(3): 243–250. [PubMed: 7994202]

21. Kim H, Booth CJ, Pinus AB, Chen P, Lee A, Qiu M, Whitlock M, Murphy PS, Constable RT. Induced hepatic fibrosis in rats: hepatic steatosis, macromolecule content, perfusion parameters, and their correlations--preliminary MR imaging in rats. Radiology. 2008; 247(3):696–705. [PubMed: 18403622]

22. Rosenkrantz AB, Storey P, Gilet AG, Niver BE, Babb JS, Hajdu CH, Lee VS. Magnetization transfer contrast-prepared MR imaging of the liver: inability to distinguish healthy from cirrhotic liver. Radiology. 2012; 262(1):136–143. [PubMed: 22114240]

23. Henkelman RM, Huang X, Xiang QS, Stanisz GJ, Swanson SD, Bronskill MJ. Quantitative interpretation of magnetization transfer. Magn Reson Med. 1993; 29(6):759–766. [PubMed: 8350718]

24. Glover GH. Simple analytic spiral K-space algorithm. Magn Reson Med. 1999; 42(2):412–415. [PubMed: 10440968]
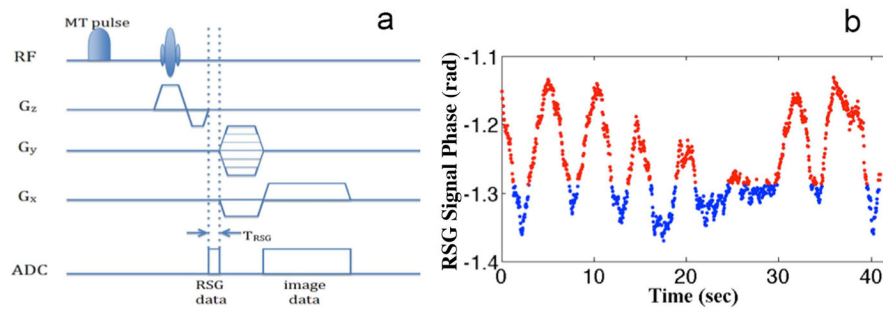
Fig. 1.
a: RSG-MT sequence diagram: a small time delay (T_{RSG}) of 80 μs was added after the slice-selective refocusing gradient. The readout prephasing gradient and phase-encoding gradient were shifted by T_{RSG} to allow eight RSG data points to be collected at k-space center before imaging data acquisition. b: A representative segment of RSG signal in rad recorded in one volunteer. The blue dots represent the RSG signal with signal phase below the local threshold corresponding to the assumed expiration position (k-space lines collected during intervals below the threshold were included in the final image reconstruction)
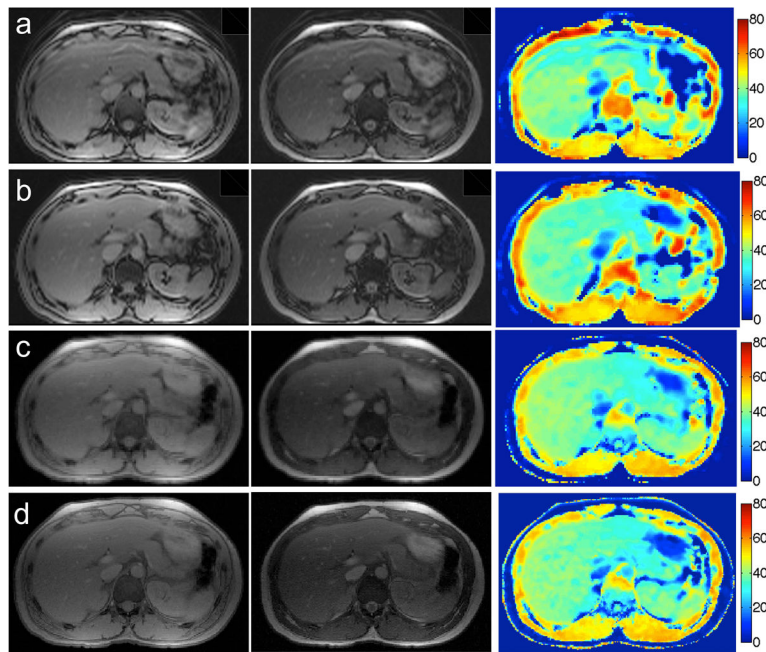
Fig. 2.
Representative images without MT saturation (left column), with MT saturation (middle column), and corresponding MTR maps (right column) in the caudal liver position acquired by using a) FB, b) BH, c) RSG, and d) high-resolution RSG MT approaches. MT saturation pulse has a FA of 900°, length of 10 ms, and off-resonance frequency of 1.5 kHz. Signal voids and blurring can be observed in the FB images with/without MT saturation. No clearly apparent motion artifacts were observed for images reconstructed from data acquired using the RSG-MT method with scanning times of more than 4 min.
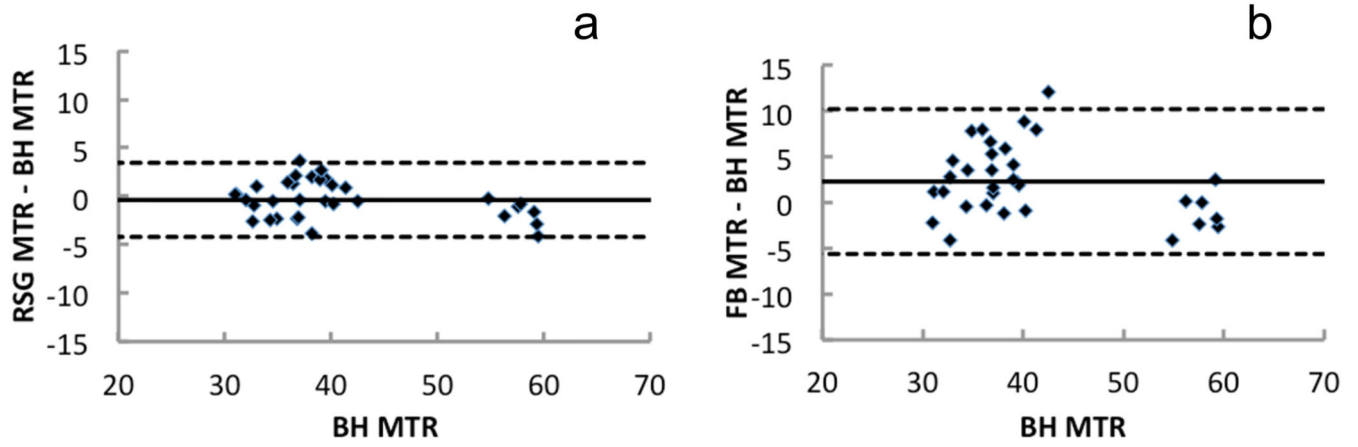
Fig. 3.
Bland–Altman plots showed that RSG MTR measurements agreed well with BH MTR measurements (a), whereas FB MTR measurements tended to overestimate MTR measurements (b).

Table 1

Mean MTR Measurements and Percentage Errors

	BH		FB		RSG	
	MTR	MTR	Percentage error (%)	MTR	Percentage error (%)	
Posterior Paraspinal Muscle	57.74±1.73	56.60±3.28	3.35±2.58	55.93±1.25	3.11±2.24
Liver	39.50±2.21	42.94±6.64	9.19±10.48	40.32±1.68	3.48±3.04
Pancreas	33.84±1.86	35.92±4.86	9.80±6.86	32.27±1.53	4.75±3.31
Kidney	36.25±2.82	40.16±5.13	11.46±7.69	35.88±3.22	4.22±3.20
Spleen	36.61±3.42	40.28±6.57	12.42±6.48	38.24±4.30	4.30±2.42